(Preprint) AAS 13-271

GRAIL SCIENCE DATA SYSTEM ORBIT DETERMINATION: APPROACH, STRATEGY, AND PERFORMANCE

Eugene Fahnestock*, Sami Asmar*, Nate Harvey*, Daniel Kahan*, Alex Konopliv*, Gerhard Kruizinga*, Kamal Oudrhiri*, Meegyeong Paik*, Ryan Park*, Dmitry Strekalov*, Dah-Ning Yuan*

This paper details orbit determination techniques and strategies employed within each stage of the larger iterative process (ref. Kruizinga et al., this meeting) of preprocessing raw GRAIL data into the gravity science measurements used within gravity field solutions. Each orbit determination pass used different data, corrections to them, and/or estimation parameters. We compare performance metrics among these passes. For example, for the primary mission, the magnitude of residuals using our orbits progressed from ≈19.4 to ≈0.077 μm/s for inter-satellite range rate data and from ≈0.4 to ≈0.1 mm/s for Doppler data.

INTRODUCTION

Orbit determination, or determining the state of each spacecraft at a chosen solution epoch (such as the start time of a data arc), is rather central to the whole of Level 1 processing as performed by the Gravity Recovery And Interior Laboratory (GRAIL) missions Science Data System (SDS) team. Here Level 1 processing means pre-processing of the raw GRAIL data into the instantaneous inter-spacecraft Ka-Band Range Rate (KBRR) gravity science measurements used within the gravity field estimation. That gravity field estimation is in turn referred to as Level 2 processing, for which the method and results are discussed separately in Park, et al. (this meeting).[1] An excellent gravity field obtained from the primary mission data alone, which has been publicly released as field GL0420A, has already demonstrated a few times improvement in spatial resolution vs. the best pre-GRAIL fields, with global (vs. lunar nearside only) coverage. It has also demonstrated 3-5 orders of magnitude (depending on harmonic degree) reduction in error vs. the best pre-GRAIL fields.[1] The GL0420A field has already enabled significant terrestrial planetary science and geophysics findings as described in a series of publications this past fall.[2,3,4]

Performing orbit determination (hereafter, OD) passes to estimate each spacecraft's epoch-state, and other parameters, is necessary in order to dynamically propagate that epoch-state and interpolate from the resulting trajectory to find the moon-centered solar system barycentric position and velocity of each of the two spacecraft, at any desired barycentric dynamical time (TDB time). This is in turn for use within computation of various corrections to the inter-spacecraft data. For example, propagation of the OD solution is done as part of producing the position and light-time information needed for the time-of-flight correction to the dual one-way range (DOWR). Another example is how propagation of the OD solution produces trajectory files used both within estimation of the

*Jet Propulsion Laboratory, California Institute of Technology, 4800 Oak Grove Drive, Pasadena CA 91109
©2013 California Institute of Technology. Government sponsorship acknowledged.

Ka-antenna boresight vector, and within calculation of the Ka-antenna phase center to mass center corrections to the DOWR for each spacecraft. Many more details are available within Reference 5.

Obtaining high-quality gravity field results required an iterative bootstrapping approach, as described in detail within Kruizinga et al. (this meeting).[6] Under this approach, after the first few Level 1 OD passes and the following data corrections, new gravity fields estimated through Level 2 processing were adopted in repeating Level 1 OD passes, to provide more accurate spacecraft ephemerides for calculating the next data corrections. After which the readjusted gravity science measurements were used for a new Level 2 gravity field estimation, and so on in alternation. In this paper we provide more detail about the techniques and strategies employed within the Level 1 OD passes, each of which used different (or differently corrected) data, different gravity fields of increasing resolution, and/or different estimation parameters.

APPROACH AND STRATEGY

General Methodology

For all of our OD, we employed the Multiple Interferometric Ranging Analysis using GPS Ensemble (MIRAGE) software, which was developed as part of the GPS Data Processing Facility (GDPF) created in support of the TOPEX/Poseidon mission. It has since been further developed for, and validated within, the highly successful GRACE mission. It is based upon the JPL legacy Orbit Determination Program (ODP),[7,8] and maintains the complete interplanetary capability of the ODP software with additional multi-satellite and precision modeling features. The version used also exploits parallel computing using MPI when advantageous, for computational tractability.

We nominally chose data arcs to process that were 36 hours in length from approximately 18:00:00 UTC on one day to 06:00:00 UTC two days later, advancing a day at a time from one arc to the next. This choice was made for operational reasons and in part to provide nominally 12 hours of overlap between successive arcs, from which we can perform an orbit overlap analysis as another metric of OD quality (see the later subsection with results from this). However, we did break arcs, with no overlap, at the center times of planned spacecraft maneuvers for which "large", i.e. ΔV >0.010 m/s, state changes were expected. These occurred frequently during the extended science mission (about once and twice per week for GRAIL-B and GRAIL-A, respectively) but only once during the primary science mission (the OTM-B2 maneuver for GRAIL-B). We did not choose to break data arcs at the smaller, as-needed maneuvers to accomplish reaction wheel angular momentum desaturations (AMDs), which typically had ΔV <0.010 m/s.

The OD using MIRAGE consisted of three major steps, and for each OD pass, for each data arc, iteration through all three steps was performed until we achieved convergence of that arc's epoch-state (and other estimated parameters) solution and convergence of that arc's observation residuals. The three steps are: 1) trajectory and partials integration, 2) observation processing, and 3) filtering. In contrast to Level 2 processing, most of the computational burden for Level 1 OD lay within the first two steps rather than the third. This is because the computational burden for the filtering step tends to be proportional to the square of the number of parameters being estimated. Fortunately a Level 1 OD pass did not involve estimation of very many parameters (i.e. <1500, for each data arc separately), unlike the Level 2 processing (e.g. >176000 parameters for a 420 degree and order lunar gravity field), and so the filtering step within each iteration was comparatively fast. Propagation of the dynamics with a higher-order gravity field still required more time, roughly proportional to the number of field coefficients, for the first two steps, which were functionally

performed together.

Thus most processing was carried out on just a single dual-node flight operations computer with 8 cores per node, such that each node could process four data arcs at once (two cores were required per arc, one for each spacecraft). Later on, as the lunar gravity field sizes increased to 660 degree and order, dilation of the time required to solve each arc plus schedule constraints prompted our porting to running on several nodes (each capable of solving four arcs at a time) on the Beowulf3 cluster at JPL.

Dynamics Modeling The equations of motion for both GRAIL spacecraft are identical in mathematical form. Below are the equations for a single spacecraft, with the understanding that the same equations apply to both spacecraft:

$$\ddot{\mathbf{r}} \;=\; \mathbf{a} \;=\; \mathbf{a}_{g_{PM}} + \mathbf{a}_{g_{oblate}} + \mathbf{a}_{srp} + \mathbf{a}_{lrp} + \mathbf{a}_{ltc} + \mathbf{a}_{rel} + \mathbf{a}_{str} + \mathbf{a}_{misc.} + \mathbf{a}_{uf}. \tag{1}$$

The fundamental reference frame in which these equations of motion are written is the non-rotating, freely-falling ("inertial") reference frame with origin defined as the center of mass of the Moon. This frame is aligned identically with the Earth Mean Equatorial J2000 frame, approximately the same as the International Celestial Reference Frame (ICRF). A lunar body-fixed frame is also employed for calculation of some of the terms on the right hand side in Eq. (1), and we use the relative orientations and associated standards for translation between this "body-fixed" frame and the "inertial frame. The independent variable for integration of the equations of motion is TDB,[9] whereas many data products are time-tagged and saved in UTC.

In Eq. (1) the subscript g_{PM} denotes point-mass gravitational accelerations for bodies other than Moon and Earth; g_{oblate} denotes gravitational accelerations due to both point-mass and higher-order than point-mass (i.e. "oblateness) gravitational fields for Moon and Earth; srp denotes acceleration due to solar radiation pressure (SRP); lrp denotes acceleration due to lunar radiation pressure, i.e. both reflected and emitted in the thermal IR incident "planetary radiation incoming from the Moon; ltc denotes acceleration due to lunar core motion and tides; rel denotes acceleration corrections due to general relativity effects; str denotes acceleration due to spacecraft thermal re-radiation; $misc.$ denotes acceleration due to miscellaneous small forces (e.g. as modeled for the AMD events); and uf denotes acceleration due to unmodeled forces, which are parameterized so that those parameters may be included among those estimated, to overcome deficiencies in the modeling of the other acceleration terms.

The total gravitational acceleration in the above is the sum of direct planetary perturbations and the lunar and Earth gravity potential perturbations. The vector of direct planetary perturbations, $\mathbf{a}_{g_{PM}}$, is evaluated as the sum of point-mass contributions of the Sun and the 7 planets other than Earth, computed using the JPL Development Ephemeris 421 (DE421) planetary masses and ephemerides. The lunar gravity potential itself is represented in a spherical harmonic representation of degree n and order m, up to a specified maximum degree and order, N_{max}, as[10]

$$U\left(r,\phi,\lambda\right) = \frac{GM_M}{r}\left[1 + \sum_{n=2}^{N_{max}}\left(\frac{R_M}{r}\right)^n \sum_{m=0}^{n} \bar{P}_{nm}\left(\sin\phi\right)\left[\bar{C}_{nm}\cos m\lambda + \bar{S}_{nm}\sin m\lambda\right]\right], \tag{2}$$

where r is the lunicentric radius and ϕ, λ are the latitude and longitude, respectively, of the field point in the lunar body-fixed frame. Note that the degree 1 terms are omitted because they are identically zero when the origin of the coordinate system is the center of mass of the planetary body

in question. The $\bar{P}_{nm}$ are normalized associated Legendre functions and the normalized coefficients $\bar{C}_{nm}, \bar{S}_{nm}$ are related to the un-normalized coefficients by[10]

$$\begin{pmatrix} \bar{C}_{nm} \\ \bar{S}_{nm} \end{pmatrix} = \sqrt{\frac{(n+m)!}{(n-m)!(2n+1)(2-\delta_{0m})}} \begin{pmatrix} C_{nm} \\ S_{nm} \end{pmatrix}, \tag{3}$$

where δ_{0m} is the Kronecker delta function. Lunar gravity acceleration is computed by evaluating the body-fixed gradient of this body-fixed gravity potential formulation, that is, the acceleration is computed as $\mathbf{a}^{bf}_{g_{oblate}} = \partial U / \partial \mathbf{r}^{bf}$. The acceleration is then rotated into the inertial frame for the integration of the equations of motion. For example

$$\mathbf{a}^{in}_{g_{oblate}} = \mathrm{M}^{in}_{bf}\left(P, N, R\right) \mathbf{a}^{bf}_{g_{oblate}}. \tag{4}$$

The 3x3 rotation matrix M^{in}_{bf}, depends on the Moon's precession P, nutation N, and polar motion R. While the above is written for the Moons gravity field, the Earths gravity field contribution is computed similarly, with truncation at significantly lower degree and order. The position of the spacecraft in the Earth-fixed frame is calculated through combination of the spacecraft state in our inertial frame of integration with the DE421 ephemeris relative position of the Earth and Moon, then rotation from the inertial to Earth-fixed frame. The same equations are applied in the Earth-fixed frame and then the resulting acceleration is rotated back into the inertial frame of integration in the same fashion as for the Moon. Values of parameters in the above equations as applied for both the Moon and the Earth are given in Table 1.

Table 1. Gravity field parameters used

Parameter	Value	Remarks
GM_M	4.902801076e+3 km^3/s^2	from DE421
R_M	1738 km	from DE421
$N_{max,M}$	210, 270, 360, 420, 540, 600, 660, etc. . . .	For fields from Level 2, but LP150Q used as original nominal field
GM_E	3.98600435600e+5 km^3/s^2	from DE421
R_E	6378.1363 km	from DE421
$N_{max,E}$	2 within OD proper, higher for precision light time calcs.	Normalized GGM02C used as nominal field

Modeling of each of the accelerations represented by the rest of the terms in Eq. (1) is described in detail within Reference 11. The development of spacecraft thermo-optical models for assistance in calculating the radiation-based terms (in particular $\mathbf{a}_{srp}$, $\mathbf{a}_{lrp}$, and $\mathbf{a}_{str}$) is described in great detail within Reference 12.

Filtering Technique Our estimation of the various parameters incorporated into the above dynamics modeling is based on the least-squares estimation principle, following after Reference 13. We define the cost function J as follows:

$$J(\mathbf{x}_0) = \frac{1}{2}\left(\mathbf{x}_0 - \mathbf{x}_a\right)^T \Lambda_a \left(\mathbf{x}_0 - \mathbf{x}_a\right) + \frac{1}{2}\left[\mathbf{z}^* - \mathbf{z}(\mathbf{x}_0)\right]^T W \left[\mathbf{z}^* - \mathbf{z}(\mathbf{x}_0)\right], \tag{5}$$

where $\mathbf{x}_0$, $\mathbf{x}_a$ are the new estimate and apriori estimate vectors of the estimated parameters, respectively, including each spacecraft's epoch-state. Also, Λ_0, Λ_a are the corresponding epoch-state and apriori information matrices, respectively, and $\mathbf{z}(\mathbf{x}_0)$, $\mathbf{z}^*$ are the computed and actual measurement vectors, respectively, while W is the measurement weight matrix. The residuals vector is identified in the above as $\Delta\mathbf{z} = \mathbf{z}^* - \mathbf{z}(\mathbf{x}_0)$. By applying the necessary conditions for optimality to the above and by linearizing about a nominal vector of estimated parameters, $\bar{\mathbf{x}}_0$, the following normal equations are obtained:

$$\left[\Lambda_a + H_{\mathbf{x}_0}^T W H_{\mathbf{x}_0}\right] \delta\mathbf{x}_0 = \Lambda_a \delta\mathbf{x}_a + H_{\mathbf{x}_0}^T W \Delta\mathbf{z}, \tag{6}$$

wherein the new estimate and apriori estimate deviation vectors (meaning deviation from the nominal vector of estimated parameters) are $\delta\mathbf{x}_0 = \mathbf{x}_0 - \bar{\mathbf{x}}_0$, and $\delta\mathbf{x}_a = \mathbf{x}_a - \bar{\mathbf{x}}_0$, respectively. Also note that the partials matrix in the above is

$$H_{\mathbf{x}_0} = \left.\frac{\partial\mathbf{z}(\mathbf{x}_0)}{\partial\mathbf{x}_0}\right|_{\mathbf{x}_0=\bar{\mathbf{x}}_0} \tag{7}$$

In Eq. (6), everything within the brackets on the left hand side is identified as the the epoch-state information matrix Λ_0, while the whole right hand size is the "data vector $\tilde{z}$. Once the epoch-state information matrix is computed, the epoch-state covariance matrix can be obtained from it simply by $P_0 = \Lambda_0^{-1}$.

The least-squares filter is an iterative method where the deviation vector, also known as the correction vector, $\delta\mathbf{x}_0$, is computed by solving these normal equations, Eq. (6), until the size of the correction vector solved for converges to within a user-defined tolerance. In the actual filtering process, MIRAGE uses the square-root information filter (SRIF) technique in order to retain numerical precision.[13] Even so, if solving for a large number of parameters, the convergence is very sensitive to the apriori parameter values and apriori parameter uncertainties. For example, if the apriori spacecraft epoch-state is poorly known, the iteration may never converge if the filter tries to solve for the trajectory and too many other additional parameters influencing the orbital dynamics at the same time.

Numerical Integration The DIVA numerical integrator[14] is used within MIRAGE to propagate the equations of motion, Eq. (1), i.e. the current spacecraft state at any time t. It is also used to propagate the state transition matrix, i.e. the matrix of partials of the current spacecraft state at any time t with respect to the epoch-state at time t_0, the latter being included in the parameters solved for. It is also used to propagate the partials of the current state at t with respect to each of the non-state parameters being estimated. When these partials and the state transition matrix are each put together, via the chain rule, with the partials of the current observations (i.e. measurements) with respect to the current state, the partials matrix $H_{\mathbf{x}_0}$ can be obtained for use in the normal equations.

DIVA is a variable order Adams method (starting out with a default order of 7) and employs a variable step size (starting with a default step size of 5 seconds, with a minimum step size of 0.0001 seconds being allowed). The step size and order are varied in order to maintain an error tolerance on the integrated state, which we at first set to 1.0×10^{-12}, and an error tolerance on the integrated partials, which we started out setting at 1.0×10^{-6}. As the resolution of the gravity field used increases, the step size determined decreases, in order to maintain fixed error tolerances. This means the span of time covered by the difference lines table in the integration method shrinks, which eventually created a problem with insufficient coverage by the difference lines table when using Doppler data with a long (60 second) compression time. This resulted in breaking the integration.

Therefore we raised the number of such difference lines from an initial 60 for the first OD passes up to 500 with the last OD passes at the time of this writing. This helped somewhat, but in addition the state and partials integration error tolerances had to be relaxed to 1.0×10^{-11} and 1.0×10^{-4}, respectively, and even then some of the one-way Doppler data had to be excluded from certain arcs. In future OD passes, switching to using different Doppler data with a shorter 10 second compression time should alleviate this issue.

Quicklook Orbit Determination

The first OD pass used only the same data available to the navigation team, i.e. closed-loop S-band two-way and closed-loop X-band one-way Doppler tracking data obtained through Deep Space Network (DSN) stations capable of both S-band uplink/downlink and X-band downlink. The former is to/from each GRAIL spacecrafts active low-gain antenna (LGA) while the latter is from each GRAIL spacecrafts active Radio Science Beacon (RSB). The compression time for this Doppler data was 60 seconds, with sampling of data points every 60 seconds within a tracking pass. We did not yet include any star-tracker-derived attitude data, and instead relied on a simplistic apriori modeling of each spacecraft's attitude. However, no vector from each spacecraft's mass center to its LGA or RSB currently in use was input, effectively assuming these antennae to be at the mass center. Thus the attitude modeling was not used after all for any kinematic correction to the Doppler data. An apriori definition of the vector from each spacecraft's mass center to its Ka-antenna's phase center was input, changing in time for each shift in mass center, with each loss of propellant mass, with each non-negligibly-sized maneuver. But in this so-called DSN-only OD pass no inter-spacecraft tracking data were yet used, so there were no data present to correct with this Ka-boresight vector plus the attitude model.

While no inter-spacecraft ranging data were yet included, we still started out with simultaneously estimating the states of both spacecraft at the arcs initial epoch. This change in methodology is the key novel development vs. the approach taken by the navigation team, who went through all navigation functions for each spacecraft separately. The apriori σ's on the three cartesian position components and three cartesian velocity components of the epoch-state for each spacecraft were initially set large (unconstrained) at 10^4 km and 10 km/s, respectively. We also concurrently estimated the following parameters, for each spacecraft:

- A solar radiation pressure scaling factor in the direction of the sun-to-spacecraft vector, applying for the whole arc, nominal value of 1.0, apriori $\sigma = 1.0 \times 10^{-2}$.
- Solar radiation pressure scaling factors in each of the two directions orthogonal to the sun-to-spacecraft vector, also applying for the whole arc, nominal values 0.0, apriori $\sigma = 5.0\times10^{-3}$.
- A bias, a drift, and a drift rate in the one-way Doppler data, applying for the whole arc (although up to 50 such biases, 50 such drifts, and 50 such drift rates could be accommodated for up to 50 "sub-arc" time periods), nominal values 0.0, apriori σ's were initially set large at 10^{20} Hz, or Hz/s, or Hz/s^2.
- Constant, once/rev, and twice/rev periodic acceleration parameters, i.e. a bias, amplitude of $\cos\theta$, amplitude of $\sin\theta$, amplitude of $\cos(2\theta)$, and amplitude of $\sin(2\theta)$, where θ means phase around the orbit, all for each component of the local radial-tangential-normal (RTN) frame, all for each sub-arc of length 6813 seconds or 6630 seconds (matching the primary mission and extended mission average orbit periods, respectively). Up to 24 such sub-arcs could be accommodated, as many as fit within the arc length. The nominal values for these

parameters were 0.0 and the apriori σ's were set to 1.0×10^{-11} km/s^2 for just the bias and once/rev parameters in just the tangential and normal components, but set to 1.0×10^{-20} km/s^2 for the rest of these periodic acceleration parameters, effectively not estimating the rest.

- The three cartesian components, with respect to the moon-centered solar system barycentric frame, of up to four accelerations due to up to four small force (thruster) events, however many actually occured within the arc's span. The nominal values were 0.0 and apriori $\sigma = 1.0 \times 10^{-5}$ km/s.

This first DSN-only pass was performed day by day as rapidly as possible after new data were downlinked, throughout the primary science mission (hereafter often abbreviated PM) and the extended science mission (similarly, XM). Hence the term "quicklook" orbit determination. It was performed for the entire PM, i.e. for arcs spanning from March 1, 2012 10:00:00 UTC to May 29, 2012 18:00:00 UTC, and the entire XM, i.e. for arcs spanning from August 30, 2012 16:00:00 UTC to December 14, 2012 21:00:00 UTC. While the set of estimated parameters and their apriori σ's were kept the same for all arcs, the gravity field used was varied, switching to higher degree and order fields as they became available over time in order to better approximate the true dynamics. This was especially needed once the spacecrafts' altitudes decreased in the XM. At first the pre-GRAIL LP150Q field[15] of 150 degree and order was used, later replaced over the course of the PM with fields from Level 2 of size 210 degree and order, then 270 degree and order, then 420 degree and order. A different and later-produced 420 degree and order field solution, the released GL0420A field, was used consistently for this pass for the whole XM.

In the second OD pass, we fit to the same data as in the DSN-only pass, but in addition fit to our first formulation of KBRR data from the GRAIL-A / GRAIL-B Lunar Gravity Ranging System (LGRS) instruments. These new KBRR data were sampled with one data point every 5 seconds for the PM, and one data point every 10 seconds for the XM. We still did not include attitude data, keeping the apriori attitude model in effect. In this second OD pass no corrections were applied to the KBRR data other than an apriori model of ultra-stable-oscillator (USO) frequency bias and drift and an apriori correction for timing error. The same apriori definition of the Ka-boresight vector as before and the same apriori attitude model as before could have been used together to correct the now present KBRR data, but that was still not done at this stage. However, definition of the locations in the spacecraft body-fixed frame for each of the two LGA and each of the two RSB antennae were now input, along with the antenna switching times specifying which LGA / RSB pair on which side of the spacecraft was active when. This information was used with the apriori attitude model within MIRAGE to apply another kinematic correction to the Doppler data.

All of the same parameters estimated in the previous DSN-only pass were estimated again within this so-called DSN + uncorrected KBRR pass, but the apriori σ's on the spacecraft position and velocity components were reduced to 1.0×10^{-2} km and 1.0×10^{-5} km/s, respectively. Also, the apriori σ's on the one-way Doppler data bias, drift, and drift rate parameters were constrained to the more reasonable 1.0×10^{2} Hz, 1.0×10^{-7} Hz/s, and 1.0×10^{-12} Hz/s^2. We then added estimation of the following parameters:

- One each of a KBRR bias, KBRR drift, KBRR cosine periodic amplitude, and KBRR sine periodic amplitude, applying for the whole arc length (although up to 50 such biases, drifts, and periodic coefficients could be accomodated for up to 50 sub-arcs). The nominal values were all set to 0.0, apriori σ's were respectively set to 1.0×10^{-7} km/s, 1.0×10^{-10} km/s^2,

and 1.0×10^{-20} km/s for the periodic amplitudes, meaning the latter were effectively not estimated.

- Up to three KBRR time tag bias parameters, with the user required to manually define any breaks within an arc separating the time intervals in which these time tag biases are to apply. No such breaks needed to be defined within the XM, but several had to be specified within certain arcs during the PM, as given in Table 2. These times are generally when the relative clock offset was reset by some event, such as a reboot of the gravity recovery processor assembly (GPA). Nominal values were 0.0 and apriori $\sigma = 100$ seconds, i.e. widely unconstrained.

The arcs were kept the same as before, and this DSN + uncorrrected KBRR pass was performed for all of the arcs day by day, as rapidly as possible after the DSN-only pass earlier that same day. The KBRR residuals plots from this provided the first solid confirmation of proper function of the payload as desired from quicklook processing. We again kept the same estimated parameters and apriori σ's between arcs, but we again varied the gravity field used between arcs to match the gravity field used for the immediately preceding DSN-only pass.

Table 2. Breakpoints defining intervals of application for multiple, successive KBRR time tag bias parameters within the same arc

arc ID	Break time (ET)	Event/Remarks
06-MAR-2012s 07-MAR-2012s	08-MAR-2012 03:48:55	GRAIL-B GPA reboot
10-APR-2012s	11-APR-2012 17:37:29	GRAIL-A GPA reboot
16-APR-2012s 17-APR-2012s	18-APR-2012 00:00:59	GRAIL-B GPA reboot
17-APR-2012s 18-APR-2012s	19-APR-2012 05:53:49	GRAIL-B GPA reboot
14-MAY-2012s 15-MAY-2012s	15-MAY-2012 06:02:00	unknown cause
15-MAY-2012s	16-MAY-2012 06:02:00	unknown cause

Final Orbit Determination

Next we fit to the same Doppler data as in the previous DSN-only and DSN + uncorrected KBRR passes, but replaced the KBRR data used in the latter with a new version of KBRR data formed from re-queried LGRS data packets (which SDS designated "version 01"). These version 01 KBRR data were sampled with one data point every 5 seconds for the PM, and one data point every 2 seconds for the XM. In addition to applying the apriori model of USO frequency bias and drift from before, these new KBRR data had applied to them corrections to adjust for: 1) Precision light time between the two spacecraft; 2) The best determined mass center to Ka-antenna phase center vectors for each spacecraft, oriented by each spacecrafts now incorporated star-tracker-derived attitude data; 3) Further timing error according to a new model. The interested reader should consult Reference 5 for details about these corrections. In addition, a similar kinematic correction to the Doppler data as

before was applied using the same LGA and RSB locations and switching times as before, but now with the real attitude data.

Many of these so-called DSN + corrected KBRR passes were performed, and in contrast to the quicklook OD, the same gravity field was used for all arcs processed in each pass. The first such pass reported herein was done using a preliminary 210 degree and order gravity field obtained by Level 2 processing using the PM's first few weeks of Doppler and version 01 KBRR data. Only arcs spanning from March 1, 2012 10:00:00 UTC to April 19, 2012 06:00:00 UTC were processed. The parameters estimated were not changed except for estimating more one-way Doppler bias, drift, and drift rate parameters, through shortening the sub-arc length in which to apply each to the average orbit period of 6813 seconds for the PM or 6630 seconds for the XM, as applicable.

The next pass reported herein was done using a 270 degree and order gravity field obtained by Level 2 processing using a few more weeks worth of the PM's Doppler and version 01 KBRR data. Only arcs spanning from March 1, 2012 10:00:00 UTC to May 09, 2012 06:00:00 UTC were processed, with no estimated parameter set changes or apriori σ changes vs. the prior pass.

The next pass reported herein was done using a 420 degree and order gravity field obtained by Level 2 processing using the entire PM's Doppler and version 01 KBRR data. All arcs spanning the whole PM from March 1, 2012 10:00:00 UTC to May 29, 2012 18:00:00 UTC were processed, again with no estimated parameter set changes or apriori σ changes. The orbit solution results from this pass were used to recompute the precision light time correction, geometric Ka-antenna phase centers separation correction, and timing corrections for the entire PM. The KBRR data formed from again re-queried LGRS data with these new corrections applied was designated "version 02" KBRR for the PM. The KBRR data sampling rates for version 02 were maintained the same as for version 01.

The next pass reported here was done using a 420 degree and order gravity field obtained by Level 2 processing using the entire PM's Doppler and version 02 KBRR data. This was the same field that was publicly released as field GL0420A. Although this field was used, the data being fit to in this pass were still the Doppler plus the version 01 KBRR data. This pass was performed for the entire PM, i.e. for arcs spanning from March 1, 2012 10:00:00 UTC to May 29, 2012 18:00:00 UTC, *and* the entire XM, i.e. for arcs spanning from August 30, 2012 16:00:00 UTC to December 14, 2012 21:00:00 UTC, though not at the same time. Again, we made no estimated parameter set changes or apriori σ changes, nor any changes to the data weighting, which had been kept constant up to and through this OD pass as 0.2 mm/s for DSN X-band one-way Doppler, 1.0 mm/s for DSN S-band two-way Doppler, and 10 μm/s for KBRR. The orbit solution results from this pass were used to recompute the same corrections mentioned above in order to create the version 02 KBRR for the XM. This version 02 KBRR generation was done about a week at a time, staggered after completion of this OD pass, throughout the XM.

We next did another DSN + corrected KBRR pass using a 540 degree and order gravity field obtained by Level 2 processing using a mix of the entire PM's Doppler and version 02 KBRR data plus the XM's Doppler and version 02 KBRR data up through October 3, 2012. Although this field was used, the data being fit to in this pass were still the Doppler and version 01 KBRR data. The entire XM from August 30, 2012 16:00:00 UTC to December 14, 2012 21:00:00 UTC was processed. There were still no changes made to estimated parameters or apriori σ's, but reflecting the smaller residuals being achieved, the data weighting was changed to a consistent 0.3 mm/s for both DSN X-band one-way and DSN S-band two-way Doppler, and 1.0 μm/s for KBRR.

We next did another DSN + corrected KBRR pass using a 660 degree and order gravity field obtained by Level 2 processing using a mix of the entire PM's Doppler and version 02 KBRR data plus the XM's Doppler and version 02 KBRR data up through October 24, 2012. However, this field was truncated to 600 degree and order before being applied in the dynamics for the equations of motion. The reason for this decision was the large power left in the harmonic error spectrum vs. the harmonic coefficients spectrum at degrees higher than 600. Although this field was used, the data fit to in this pass were still the Doppler and version 01 KBRR data. For logistical reasons, only the arcs of the XM spanning from November 6, 2012 18:00:00 UTC to December 14, 2012 21:00:00 UTC were processed in this pass. There were still no changes made to estimated parameters, apriori σ's, or data weighting with respect to the previous pass described.

Finally, after GRAIL concluded with the intentional crashing of both spacecraft into the lunar surface, two more DSN + corrected KBRR passes were performed. This time the data fit to were the Doppler and version 02 KBRR data, for both passes. The first of these was done using an improved 660 degree and order gravity field, without any truncation, obtained by Level 2 processing using *only* the PM's Doppler and version 02 KBRR data. This pass was performed for only the arcs spanning the PM. There were still no changes made to estimated parameters or apriori σ's, but the data weighting was again revised to 0.3 mm/s for all Doppler data but just 0.06 μm/s for KBRR data during the PM.

The last pass was done using a 660 degree and order gravity field, again without any truncation, obtained by Level 2 processing using *both* the PM's and XM's Doppler and version 02 KBRR data. This pass was performed for all arcs spanning both the PM and XM, with no further changes to parameterization or data weighting except that the version 02 KBRR data for the XM was down-weighted vs. that for the PM, at 0.2 μm/s up until October 3, 2012, and 1.0 μm/s after that date. The 0.06 μm/s weight was still used for the PM. For some arcs nearing the end of the XM during which the lowest altitudes were achieved, using this gravity field led to the numerical integration problems mentioned earlier. Even after attempting increasing the maximum number of difference table lines and increasing the error tolerances, these problems were often solved only by excluding all one-way Doppler data from the fitting for these arcs. Curiously, the two-way Doppler data never needed to be excluded in the same way. The orbit solutions of this OD pass are being used to create version 03 of the KBRR data, for further iteration between Level 1 and Level 2 processing.

PERFORMANCE

In this section, we present selected results for the OD passes described in the last section. In particular, we compare four major types of performance metrics for the orbits obtained: Doppler data residuals, KBRR data residuals, the KBRR data time tag bias parameter estimates, and orbit overlap statistics.

Doppler Data Residuals

The postfit residuals of the DSN Doppler data fitted reveal how well our GRAIL orbits were determined relative to the inertial frame. For the PM, the average and maximum (each taken over all arcs processed in a given OD pass) of the per-arc postfit RMS residuals for all DSN Doppler data progressed from $\approx$0.4 and $\approx$1.2 mm/s with our first DSN + corrected KBRR pass described earlier, down to $\approx$0.1 and $\approx$0.5 mm/s with our DSN + corrected KBRR pass using GL0420A. Minimal additional improvement, to $\approx$0.1 and $\approx$0.3 mm/s, was realized by the last DSN + corrected KBRR pass described earlier. Figure 1 shows the comparison between the latter two solutions, broken

down by spacecraft and Doppler type. The Level 2 processing local solutions,[1] exhibited ≈0.1 mm/s average RMS residuals for two-way Doppler over the PM, to which the results herein compare well.

For the XM, the average and maximum of per-arc postfit RMS residuals for all DSN Doppler data progressed from ≈1.6 and ≈12.5 mm/s with the DSN + corrected KBRR pass using GL0420A down to ≈0.2 and ≈0.7 mm/s with the last DSN + corrected KBRR pass described earlier. Figure 2 shows the comparison between these two solutions. Note the same two OD passes with the same two fields are being compared in Figure 2 as in Figure 1, but the improvement was much greater for the XM.

We originally intended to also compare in this paper the results from repeating our last DSN + corrected KBRR pass after switching from the closed-loop X-band one-way Doppler data mentioned earlier to open-loop X-band one-way Doppler data received from the RSB on each spacecraft by Radio Science Receivers (RSRs) installed only at DSN stations 15, 24, 34, 45, 54, 55, and 65. These RSR data, once properly adjusted, should generally be lower in noise than the counterpart closed-loop data they replace, allowing us to adjust weighting and achieve some improvement in the fits performance. However, at the time of this writing, work is ongoing to resolve several remaining problems with the RSR data that prevent it from being usable.

KBRR Data Residuals

The postfit residuals of the KBRR data fitted reveal how well our GRAIL orbits for each spacecraft were determined relative to each other and relative to the true gravity field in the lunar body-fixed frame. For the PM, the average and maximum of per-arc postfit RMS residuals for KBRR progressed from ≈19.4 and ≈82.4 μm/s with the DSN + uncorrected KBRR pass down to ≈0.077 and ≈0.164 μm/s with the last DSN + corrected KBRR pass described earlier. This dramatic improvement is shown in Figure 3. The ≈0.05 μm/s achieved during the most dynamically quiet (in terms of non-gravitational perturbations) central period of the PM agrees very well with the JPL Level 2 processing solutions reported this meeting.[1]

For the significantly different orbital geometry of the XM, the average and maximum of per-arc postfit RMS residuals for KBRR progressed from ≈18.6 and ≈113 μm/s with the DSN + corrected KBRR pass using GL0420A down to ≈0.88 and ≈6.28 μm/s with the last DSN + corrected KBRR pass. This is illustrated in Figure 4. The degradation remaining from November 17, 2012 onward points toward the need for more OD passes using the version 03 KBRR.

KBRR Data Time Tag Biases

For the PM, the KBRR time tag bias estimate at first had large variations from arc to arc ranging between ±30 milliseconds (See Figure 5, panel (a), the black and blue curves). As we performed the DSN + corrected KBRR passes using gravity fields of 270 and then 420 degree and order, these variations smoothed out significantly to reveal linear trends over each of four distinct periods separated by the events detailed in the first four lines of Table 2. An additional outlier in the time tag estimate remained remained for the arc 15-MAY-2012s spanning the undetermined glitches in the last two lines of this table. Prior to generating version 02 KBRR data, changes were made to the software for computing timing corrections to the KBRR data, in order to compensate for these events. Thus in the OD passes performed using GL0420A and thereafter, the KBRR time tag estimates varied by ¡ 1 millisecond about the mean value across all arcs (which was 1020.67 milliseconds for the last DSN + corrected KBRR pass reported herein). This behavior is seen in Figure 5, panel (b).

For the XM, the KBRR time tag bias estimate started out having large variations with roughly bi-weekly occurrence, reaching 26 and +120 milliseconds, with the DSN + corrected KBRR pass using GL0420A (see Figure 6). The excursions seemed to be correlated with epochs when the GRAIL orbits were face-on with respect to the Earth. The KBRR time tag bias estimate improved greatly until, for the last DSN + corrected KBRR pass reported herein, only small random variations of <6 milliseconds remained about a shallowly rising trendline from 49.9965 milliseconds (first arc) to 52.5935 milliseconds (last arc). Most variations from this trend were much smaller, with the 08-DEC-2012s arc being a noticeable outlier. Several GPA reboot events also occurred and had to be compensated for during the XM, including on this day.

Orbit Overlap Statistics

As another metric of orbit determination quality, for each spacecraft we calculated the RSS of the difference between adjacent and overlapping arcs in each RTN frame component of the spacecraft position, sampled every 5 seconds over the nominal 12 hour arc overlap period. Such an overlap period existed only if the adjacent arcs were not beginning/ending at a common time of a maneuver. For the PM, the orbit overlap statistics thus obtained started out poorly, reaching up to 13 m, up to 230 m, and up to 260 m in radial, along-track, and cross-track, respectively. The same metrics improved to no more than 0.2 m, 2 m, and 0.7 m in radial, along-track, and cross-track, respectively, with the DSN + corrected KBRR pass using GL0420A. Figure **??** shows that minimal further improvement resulted in going from those orbit solutions to orbit solutions with the last DSN + corrected KBRR pass reported herein. Like the Doppler data residuals results, this suggests that the PM was already mostly converged, in the sense of the larger iteration between Level 1 and Level 2 processing, before the start of the XM.

In contrast, again like the Doppler data residuals results, for the XM a large improvement was made between the same two OD passes: the same orbit overlap metrics went from up to 30 m in radial and cross-track and up to 150 m in along-track, down to no more than 0.8 m, 9.5 m, and 1.2 m in radial, along-track, and cross-track, respectively. This is shown in Figure 8, for which the vertical scales had to be adjusted between panels. This large improvement, as for the Doppler data residuals results, reflects how much further the bootstrapping needed to go to accommodate the lower-altitude data of the XM.

SUMMARY

We would like to emphasize that the key aspects of our approach enabling the progression to such a high level of orbit determination quality as shown above were: 1) concurrently estimating the states of the two spacecraft together; 2) the combination of such an excellent set of KBRR data for relative spacecraft motion observability and Doppler data for the orbits' absolute motion, or inertial frame tie, observability; and 3) the larger bootstrapping process involving iteration of these OD passes with determination of increasingly high degree and order gravity fields. As for the third item, at the time of this writing a few more iterations are planned to be made, involving a few additional OD passes using the version 03 (and higher versions) of KBRR data, and also using new gravity fields of >700 degree and order solved for using the version 03 (and higher) KBRR data. While we appear to have already nearly converged to the noise floor of the data for the primary mission, or at least the most dynamically quiet central portion of it, such convergence is yet to be achieved for the last month or so of the extended mission.

ACKNOWLEDGMENTS

The work described in this paper was carried out at the Jet Propulsion Laboratory, California Institute of Technology, under a contract with the National Aeronautics and Space Administration. The authors are members of the GRAIL Science Data System team, which is part of the GRAIL project. We would like to acknowledge the support from the rest of the GRAIL project at large, and especially the interchange with the Mission Design, Navigation, and Mission Operations teams.

REFERENCES

[1] R. Park, A. Konopliv, D.-N. Yuan, S. Asmar, E. Fahnestock, G. Kruizinga, M. Paik, M. Watkins, D. Smith, and M. Zuber, "High-Resolution Lunar Gravity from the Gravity Recovery And Interior Laboratory Mission," *presented at the 23rd AAS/AIAA Spaceflight Mechanics Meeting*, paper AAS 13-272, Lihue, Hawaii, USA, February 10–14, 2013.

[2] M. T. Zuber, D. E. Smith, M. M. Watkins, S. W. Asmar, A. S. Konopliv, F. G. Lemoine, H. J. Melosh, G. A. Neumann, R. J. Phillips, S. C. Solomon, M. A. Wieczorek, J. G. Williams, S. J. Goossens, G. Kruizinga, E. Mazarico, R. S. Park, and D.-N. Yuan, "Gravity Field of the Moon from the Gravity Recovery and Interior Laboratory (GRAIL) Mission," *ScienceExpress*, December 5, 2012.

[3] M. A. Wieczorek, G. A. Neumann, F. Nimmo, W. S. Kiefer, G. J. Taylor, H. J. Melosh, R. J. Phillips, S. C. Solomon, J. C. Andrews-Hanna, S. W. Asmar, A. S. Konopliv, F. G. Lemoine, D. E. Smith, M. M. Watkins, J. G. Williams, and M. T. Zuber, "The Crust of the Moon as Seen by GRAIL," *ScienceExpress*, December 5, 2012.

[4] J. C. Andrews-Hanna, S. W. Asmar, J. W. H. III, W. S. Kiefer, A. S. Konopliv, F. G. Lemoine, I. Matsuyama, E. Mazarico, P. J. McGovern, H. J. Melosh, G. A. Neumann, F. Nimmo, . D. E. S. Roger J. Phillips, S. C. Solomon, G. J. Taylor, M. A. Wieczorek, J. G. Williams, and M. T. Zuber, "Ancient Igneous Intrusions and Early Expansion of the Moon Revealed by GRAIL Gravity Gradiometry," *ScienceExpress*, December 5, 2012.

[5] N. Harvey, E. Fahnestock, D. Kahan, A. Konopliv, G. Kruizinga, K. Oudrhiri, M. Paik, D.-N. Yuan, S. Asmar, and M. Watkins, "GRAIL Level-1 Algorithm Theoretical Basis Document," Tech. Rep. JPL D-75862, Jet Propulsion Laboratory, California Institude of Technology, Pasadena, CA, USA, 2012.

[6] G. Kruizinga, S. Asmar, E. Fahnestock, N. Harvey, D. Kahan, A. Konopliv, K. Oudrhiri, M. Paik, R. Park, D. Strekalov, M. Watkins, and D.-N. Yuan, "The Role of GRAIL Orbit Determination in Pre-Processing of Gravity Science Measurements," *presented at the 23rd AAS/AIAA Spaceflight Mechanics Meeting*, paper AAS 13-270, Lihue, Hawaii, USA, February 10–14, 2013.

[7] T. D. Moyer, *Mathematical Formulation of the Double-Precision Orbit Determination Program (DPODP)*. JPL Technical Report 32-1527, Pasadena, CA, USA: Jet Propulsion Laboratory, California Institute of Technology, 1971.

[8] T. D. Moyer, *Formulation for Observed and Computed Values of Deep Space Network Data Types for Navigation*. No. 2 in Deep Space Communications And Navigation Series Monographs, Pasadena, CA, USA: Jet Propulsion Laboratory, California Institute of Technology, 2000.

[9] G. Petit and B. Luzum, eds., *IERS Conventions (2010)*. No. 36 in IERS Technical Notes, Frankfurt am Main, Germany: International Earth Rotation and Reference Systems Service (IERS), Central Bureau, Bundesamt für Kartographie und Geodäsie, 2010.

[10] W. M. Kaula, *Theory of Satellite Geodesy: Applications of Satellites to Geodesy*. New York: Dover, 2000.

[11] R. S. Park, S. W. Asmar, E. G. Fahnestock, A. S. Konopliv, W. Lu, and M. M. Watkins, "Gravity Recovery and Interior Laboratory Simulations of Static and Temporal Gravity Field," *Journal of Spacecraft and Rockets*, Vol. 49, No. 2, 2012, pp. 390–400.

[12] E. G. Fahnestock, R. S. Park, D.-N. Yuan, and A. S. Konopliv, "Spacecraft Thermal And Optical Modeling Impacts on Estimation Of The GRAIL Lunar Gravity Field," *Proc. AIAA/AAS Astrodynamics Specialist Conference*, paper AIAA 2012-4428, Minneapolis, Minnesota, USA, August 13–16, 2012.

[13] G. J. Bierman, *Factorization Methods for Discrete Sequential Estimation*. New York: Academic Press, 1977.

[14] F. T. Krogh, "Changing Stepsize in the Integration of Differential Equations Using Modified Divided Differences," JPL Technical Memo, No. 312, Section 914 (internal document), Jet Propulsion Laboratory, California Institute of Technology, Pasadena, CA, USA, 1973.

[15] A. S. Konopliv, S. W. Asmar, E. Carranza, W. L. Sjogren, and D.-N. Yuan, "Recent Gravity Models as a Result of the Lunar Prospector Mission," *Icarus*, Vol. 150, No. 1, 2001, pp. 1–18.

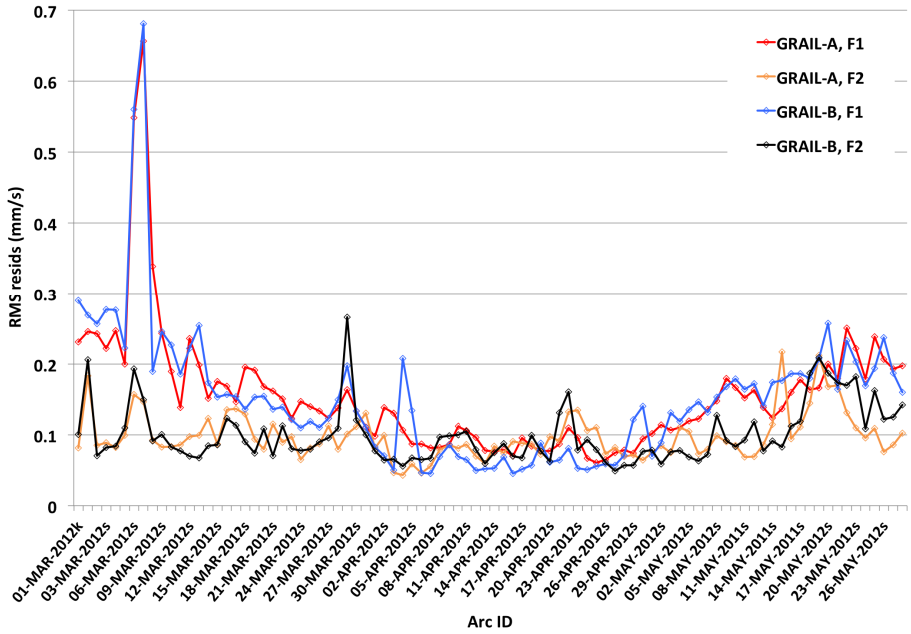

(a) for the DSN + corrected KBRR pass using GL0420A

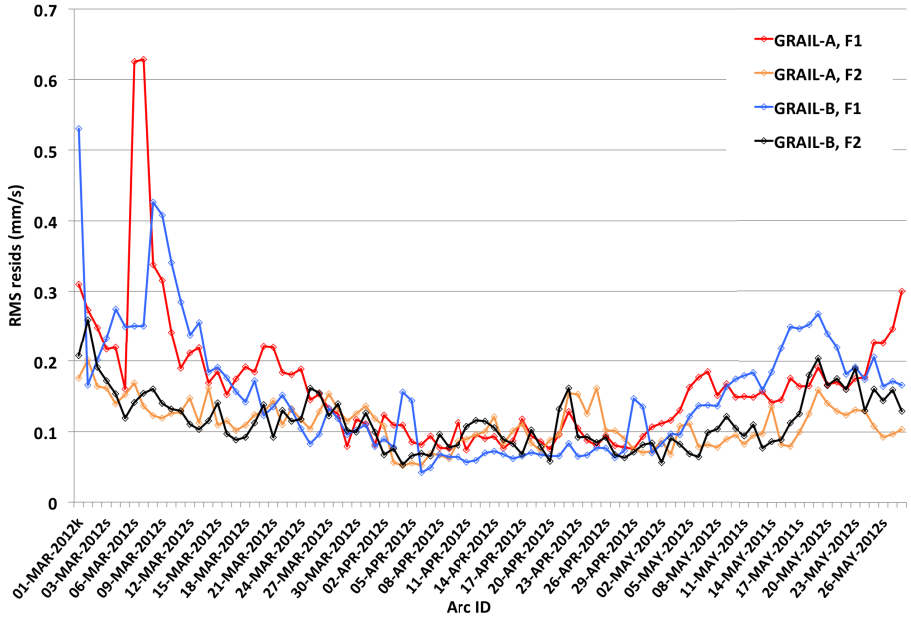

(b) for the DSN + corrected KBRR pass using the 660×660 field from both PM and XM last described in the text

Figure 1. Comparison of per-arc DSN Doppler RMS residuals for the primary mission. Here F1 denotes one-way Doppler, F2 denotes two-way Doppler.

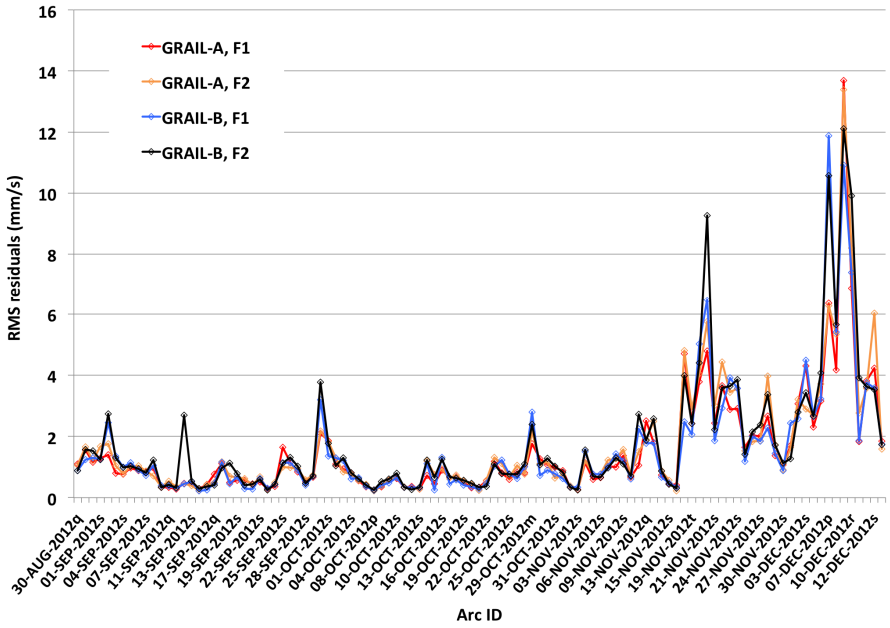

(a) for the DSN + corrected KBRR pass using GL0420A

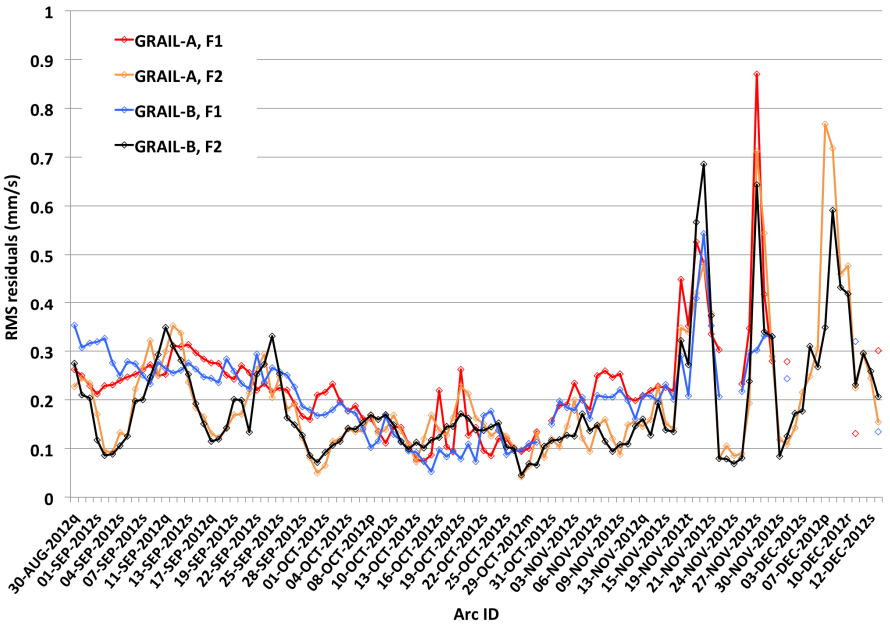

(b) for the DSN + corrected KBRR pass using the 660×660 field from both PM and XM last described in the text

Figure 2. Comparison of per-arc DSN Doppler RMS residuals for the extended mission. Here F1 denotes one-way Doppler, F2 denotes two-way Doppler.

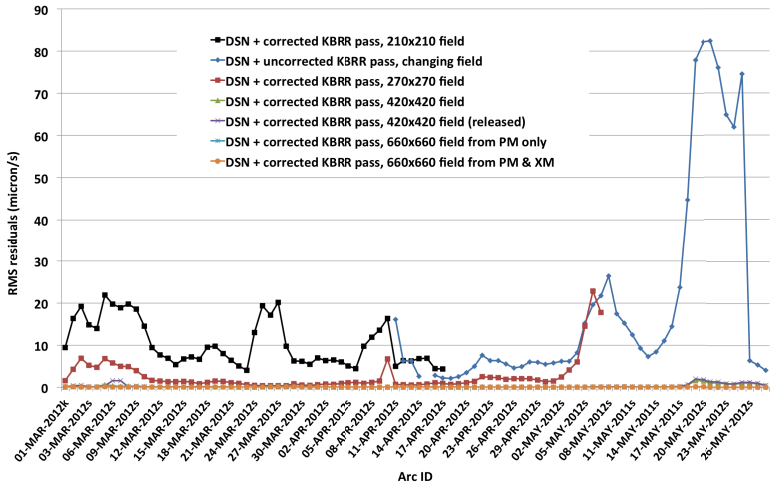

(a)

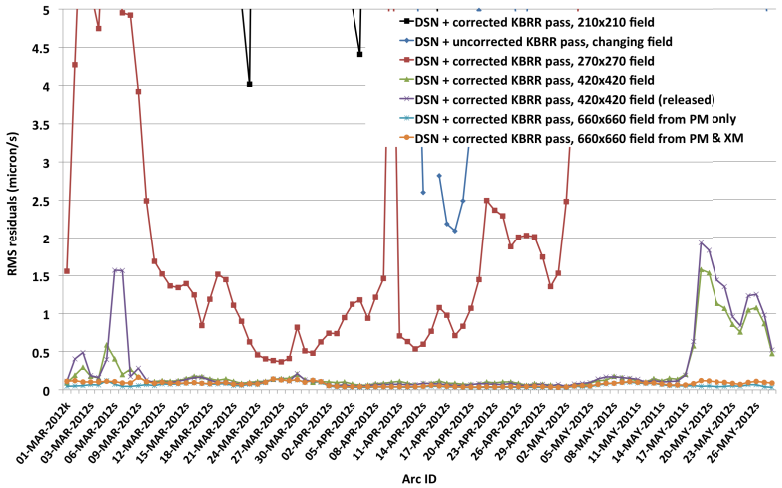

(b)

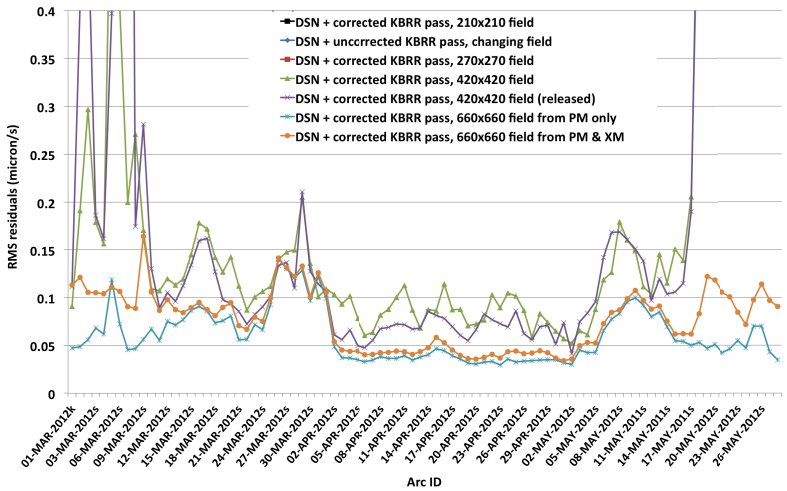

(c)

Figure 3. Progression of per-arc KBRR RMS residuals for successive OD passes conducted for primary mission through January 2013. Panels (b) and (c) are the same as (a) but with the vertical scale zoomed by 18x and 225x, respectively.

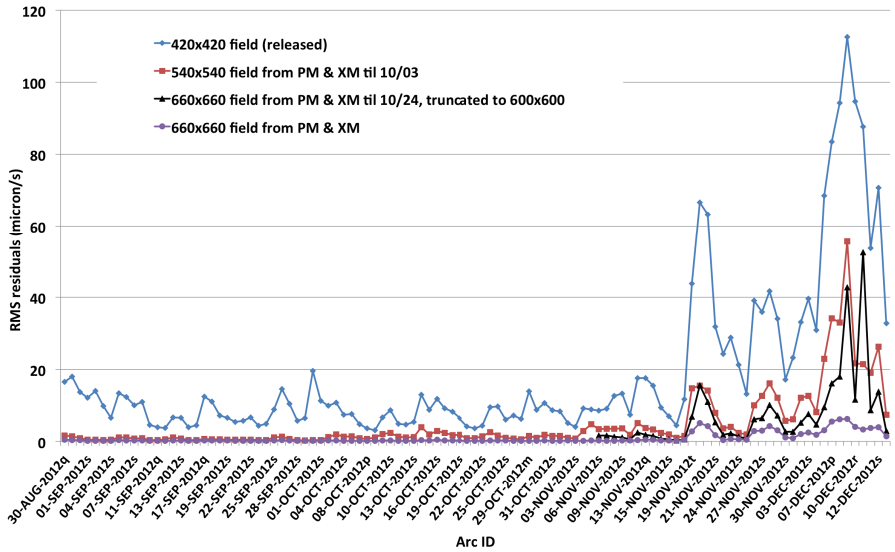

(a)

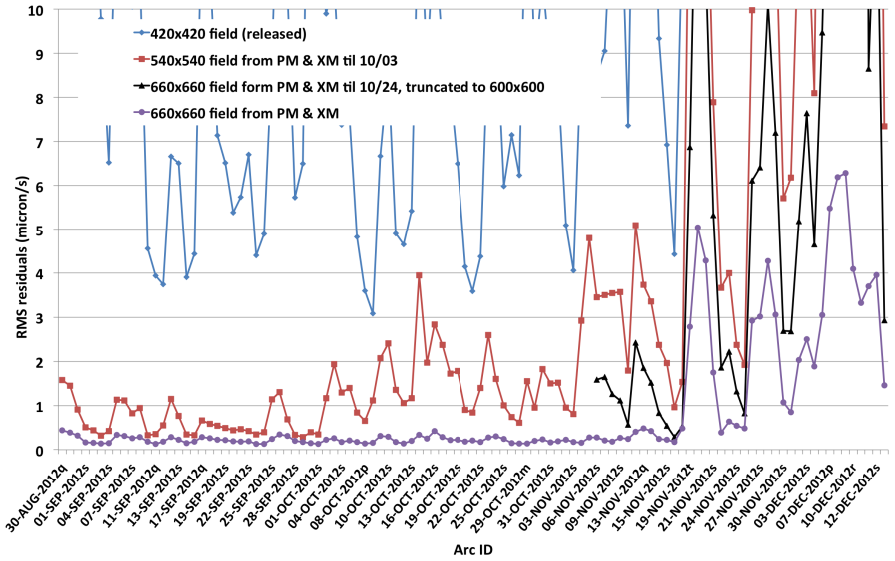

(b)

Figure 4. Progression of per-arc KBRR RMS residuals for successive OD passes conducted for extended mission through January 2013. Panel (b) is the same as panel (a) but with the vertical scale zoomed by 12x.

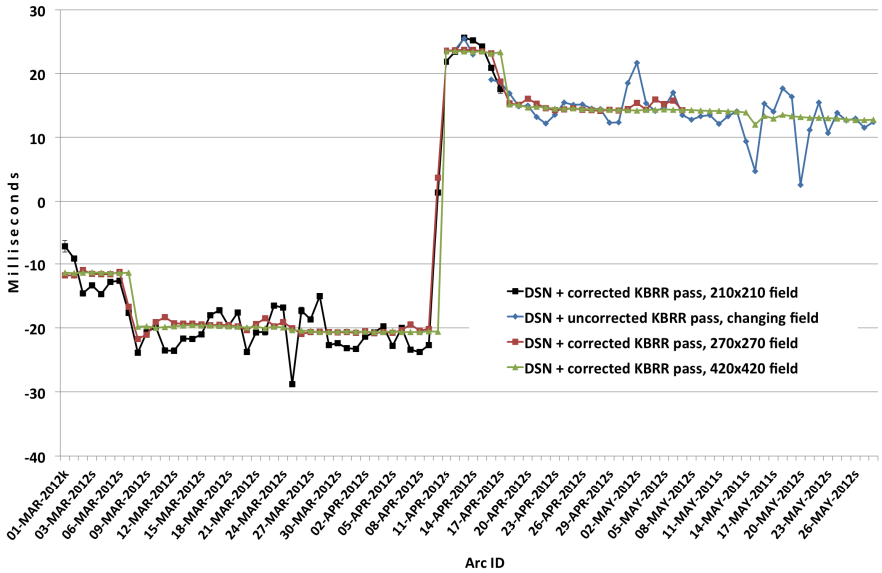

(a)

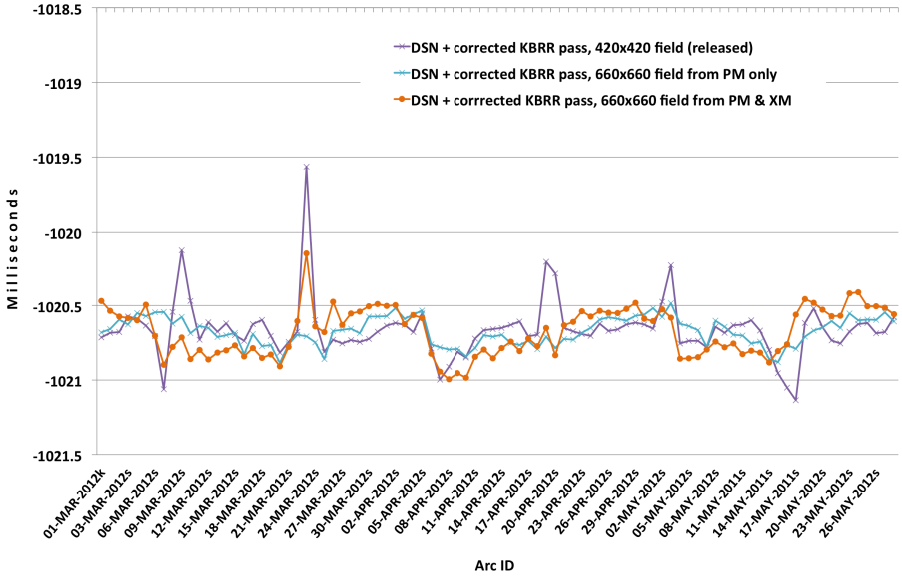

(b)

Figure 5. Progression of per-arc KBRR time tag bias estimates for successive OD passes conducted for primary mission through January 2013. Note panel (b) shows solutions after introduction of changes to the timing correction software (see text).

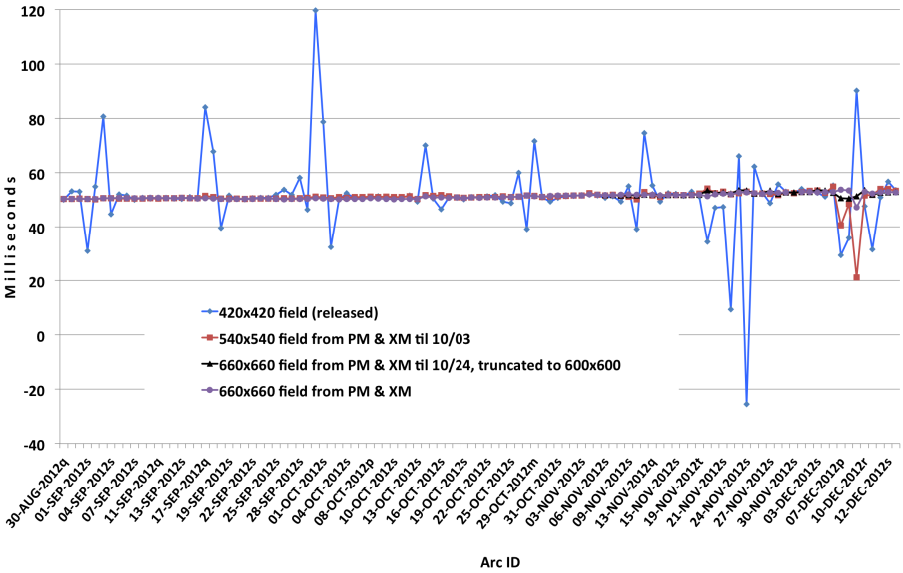

Figure 6. Progression of per-arc KBRR time tag bias estimates for successive OD passes conducted for extended mission through January 2013.

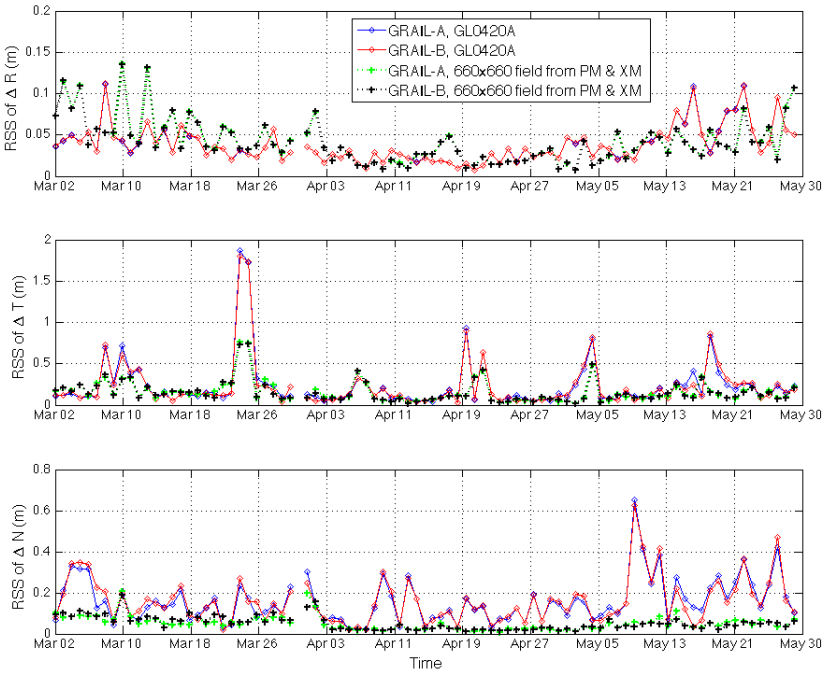

Figure 7. Comparison of per-arc orbit overlap statistics for final OD passes using GL0420A vs. the 660×660 field from both PM and XM last described in the text, for the primary mission.

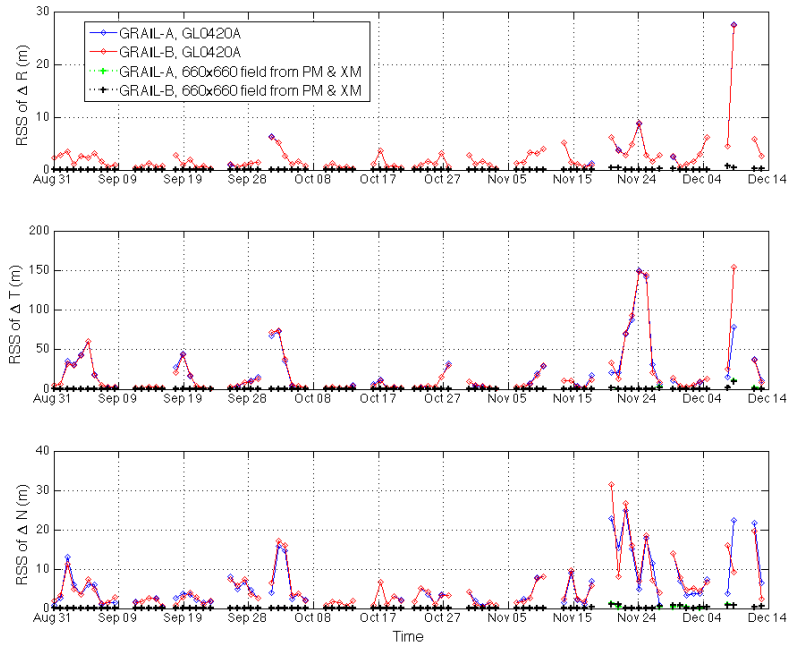

(a)

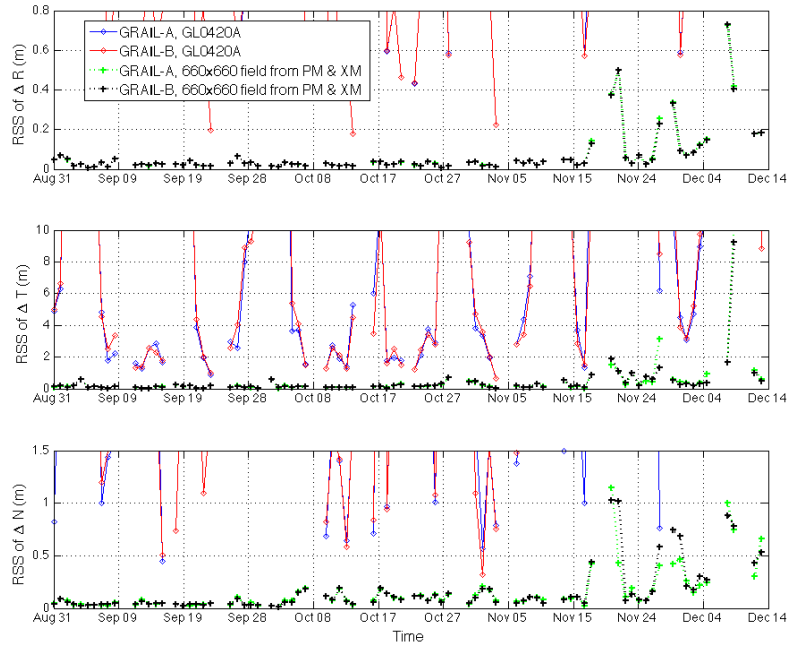

(b)

Figure 8. Comparison of per-arc orbit overlap statistics for final OD passes using GL0420A vs. the 660×660 field from both PM and XM last described in the text, for the extended mission. Panel (b) is identical to panel (a) except for the vertical axes in each component being zoomed to better show the latter OD pass's results.